



1 *Conference Proceedings Paper*

2 **Classification of Sentinel-2 Images Utilizing** 3 **Abundances Representation**

4 **Eleftheria Mylona** ^{1,*}, **Vassiliki Daskalopoulou** ¹, **Olga Sykioti** ¹, **Konstantinos Koutroumbas** ¹,
5 **Athanasios Rontogiannis** ¹

6 ¹ Institute of Astronomy, Astrophysics, Space Applications and Remote Sensing, National Observatory of
7 Athens; emylona@noa.gr, vdaskalop@noa.gr, sykioti@noa.gr, koutroum@noa.gr, tronto@noa.gr.

8 * Correspondence: emylona@noa.gr; Tel.: +30-2108109195

9 Published: date

10 Academic Editor: name

11 **Abstract:** This paper deals with (both supervised and unsupervised) classification in multispectral
12 Sentinel-2 images, utilizing the abundances representation of the pixels of interest. The latter pixel
13 representation uncovers the hidden structured regions which are not often available in the reference
14 maps. Additionally, it encourages class distinctions and bolsters accuracy. The adopted
15 methodology, which has been successfully applied on hyperpsectral data involves two main
16 stages: (I) the determination of the pixels abundance representation and (II) the employment of a
17 classification algorithm applied on the abundance representations. More specific, stage (I)
18 incorporates two key processes namely: (a) **endmember extraction** utilizing spectrally
19 homogeneous regions of interest (*ROIs*) and, (b) **spectral unmixing**, which hinges upon the
20 endmember selection. The adopted spectral unmixing process assumes the Linear Mixing Model
21 (*LMM*), where each pixel is expressed as a linear combination of the endmembers. The pixel's
22 abundance vector is estimated via a variational Bayes algorithm that is based on a suitably defined
23 hierarchical Bayesian model. The resulting abundance vectors are then fed to stage (II) where two
24 off-the-shelf supervised classification approaches (namely nearest neighbor (*NN*) classification and
25 support vector machines (*SVM*)) as well as an unsupervised classification process (namely online
26 adaptive possibilistic c-means (*OAPCM*) clustering algorithm), are adopted. Experiments are
27 performed on a Sentinel-2 image acquired for a specific region of the Northern Pindos National Park
28 in the northwestern Greece containing water, vegetation and bare soil areas. The experimental
29 results demonstrate that the ad-hoc classification approaches utilizing the abundance
30 representations of the pixels outperform the ones utilizing the spectral signatures of the pixels, in
31 terms of accuracy.

32 **Keywords:** spectral unmixing; classification; clustering; Sentinel-2 imagery; land cover.
33

34 **1. Introduction**

35 Land cover analysis and classification is essential for various environmental and mapping
36 applications. Land classification yields to thematic maps which integrate land cover materials.
37 Sentinel-2 data has gained leverage in the remote sensing community due to the high spatial and the
38 high temporal resolution. Sentinel-2 multispectral high-resolution sensor (*MSI*) operates on thirteen
39 different bands of which four have a resolution of ten meters, six a resolution of twenty meters and
40 three a resolution of sixty meters. Hence, Sentinel-2 data provide information on the reflectance of
41 the land surface for many different wavelengths on a local and regional scale. Regardless of the

42 sensor's spectral resolution, these images are challenged by the presence of mixed pixels, which
43 depict mixtures of distinct materials.

44 Each mixed pixel is associated with the electromagnetic reflection of various materials measured
45 in numerous spectral bands belonging to the surface depicted by the pixel, measured in numerous
46 spectral bands. These measurements constitute the spectral signature of the pixel. Two processes are
47 fundamental in analysis such as: (a) the detection of the constituent components of mixed pixels as
48 well as the proportions in which they appear and, (b) the identification of homogeneous regions. The
49 first objective is tackled via spectral unmixing and the second via the use of classification algorithms.

50 Classification [1]-[4] partitions the set of pixels from the input image into compact, homogeneous
51 groups. It is performed in either supervised or unsupervised way usually operating in the spectral
52 signatures of the pixels. Hitherto, mixed surface features are tackled by supervised classification
53 approaches, which require the availability of a labeled set of pixels. These pixels form the training set
54 that is used for teaching the classifier the underlying pixel classification task in order to further
55 classify the unlabeled pixels. Popular classification methods proposed in literature include the
56 nearest neighbor classifier [5],[6] and the support vector machines (SVMs) [7].

57 Several classification methods have been applied on Sentinel-2 images. In this work we assess
58 the performance of a recently proposed classification method [2], originally proposed for
59 hyperspectral images on Sentinel-2 data. The main idea of the methodology is to perform first spectral
60 unmixing based on a suitably selected set of endmembers and represent each pixel by its associate
61 abundance vector (constituted from the corresponding abundance values). Then, the classification
62 of the pixels is performed on the abundance vectors of the pixels and not on their spectral signatures
63 (actually two supervised and one unsupervised classification algorithms are utilized). To assess the
64 performance of the adopted methodology on Sentinel-2 data, we compare with the case where
65 spectral signature pixel representations are considered. To the best of our knowledge this is the first
66 attempt of utilizing a combination of both spectral unmixing and classification tasks on Sentinel-2
67 data.

68 The area on which the methodology will be assessed is that of Northern Pindos National Park-
69 Greece (Sentinel-2 data). Section 2 describes the adopted algorithm. Section 3 demonstrates the results
70 obtained by ad-hoc classification algorithms utilizing the spectral signatures and the abundances
71 representations. Conclusion is summarized in Section 4.

72 **2. Methods**

73 *2.1 Test Area*

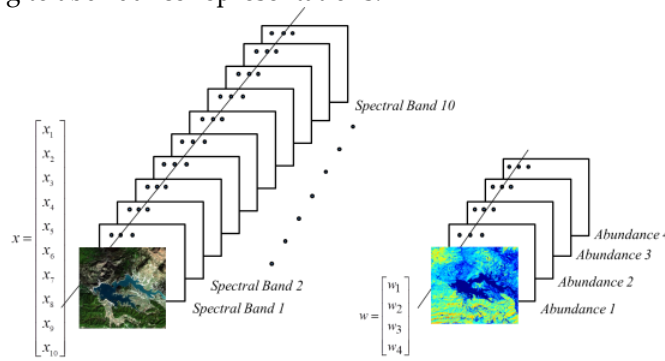
74 The test area is a specified region of the Northern Pindos National Park in the northwestern
75 Greece. This region is the largest protected forestry region with high topographical diversity. The
76 image has a resolution of 30m consisting of 333×333 pixels and is depicted in Fig. 4(a). We utilized
77 the image at 30m resolution instead of the one at 10m resolution in order to compare the results
78 obtained by the proposed algorithm with the reference classification map provided at 30m resolution
79 [6]. The image depicts the artificial lake of Aoo on the northwest of Metsovo and a small part of the
80 mountains of Pindos. The region is dominated by grassland, prickly oaks and hornbeams, beech,
81 black pine and deciduous oak. The verge of the mountain slopes is covered by Bosnian pine. Human
82 agricultural activities are also present along the water basin. The image is atmospherically corrected
83 and this process yielded to the reduction of the number of bands from 13 to 10, namely band 1 (443
84 nm), band 9 (945 nm) and band 10 (1375 nm) have been removed. Four basic classes, namely Water,
85 Dense Vegetation, Soil and Sparse Vegetation are specified.

86 *2.2 Adopted Methodology*

87 The adopted methodology is motivated by the properties of the abundances of ground materials
88 present in the pixels of a Sentinel-2 image. Each pixel is represented by a vector of ten spectral bands
89 and the original space is reshaped to the dimensionally reduced space of abundances. (see Figure 1).

90 In addition, since the abundance representation of a pixel unveils sub-pixel level information, this
91 allows the proposed algorithm to identify possible refined structures within each region, which is
92 usually not available in the ground truth maps.

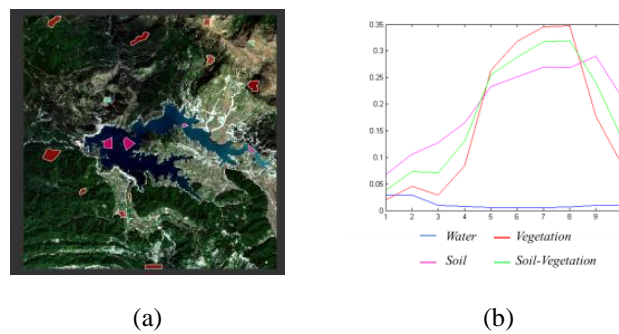
93 The scope is to employ first endmember extraction (*EE*) by identifying spectrally homogeneous
94 regions (regions of interest, *ROIs*) and extracting the mean endmembers of the image based on the
95 collected *ROIs*. Secondly, it employs a *SU* method that is based on the endmembers extracted by *EE*,
96 in order to produce the abundance fractions for each pixel, which in turn form the so-called
97 abundance vector of the pixel. These vectors from all pixels are fed to the classification process that
98 groups pixels according to abundance representations.



99
100 **Figure 1.** Spectral bands from the original spectral band space are dimensionally reduced to the less
101 correlated abundance space.

102 2.2.3. A. *EE*

103 Aiming at selecting representative endmembers for each class, suitable regions of interest (*ROIs*)
104 were selected. In our experiments we use four main land cover classes, namely (a) Water, (b) Dense
105 Vegetation, (c) Soil and (d) Sparse Vegetation. All endmembers are calculated as the average values
106 of the spectral signatures of the pixels in each *ROI*. Figure 2 depicts (a) the appropriate *ROIs* selected
107 on the Sentinel-2 image (*see* Section 3: Fig. 4(a)), (b) the endmembers of four main classes, water, dense
108 vegetation, soil, sparse vegetation.



109 **Figure 2.** (a) *ROIs* selection for endmember extraction, (b) endmembers of four classes, water, dense
110 vegetation, soil, sparse vegetation.

111
112 2.2.4. B. *SU*

113 The selection of appropriate endmembers is crucial so as to correctly estimate the abundance
114 fractions. The spectral signature of the pixel, denoted by x , is assumed to follow the Linear Mixing
115 Model (*LMM*). The latter adopts the hypothesis that the spectrum of a mixed pixel is a linear
116 combination of its endmembers' spectra as follows:

117
118
$$x = \Phi w + n \tag{1}$$

119

120 where $\Phi = [\phi_1, \phi_2, \dots, \phi_p] \in \mathbb{R}_+^{L \times p}$, $L \gg p$, is the mixing matrix comprising the endmembers'
121 spectra in its columns (L -dimensional vectors $\phi_i, i=1, 2, \dots, p$), w is a $p \times 1$ vector consisting of the
122 corresponding abundance fractions, named abundance vector, and n is an $L \times 1$ additive noise
123 vector, which is assumed to be a zero-mean Gaussian distributed random vector with independent
124 and identically distributed elements.

125 The abundance fractions for each pixel should be non-negative and sum to one. The abundance
126 vector for each pixel is estimated via a variational Bayes algorithm, called *BiICE* which is based on an
127 appropriately defined hierarchical Bayesian model [8]. In algorithmic form the abundance vector can
128 be written as:

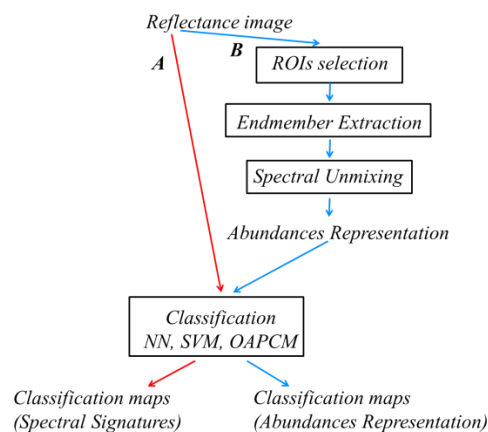
129 $w = \text{BiICE}(\Phi, x).$

130 *BiICE* is computationally efficient, provides sparse solutions without requiring the fine-tuning
131 of any parameters and converges fast to accurate values even for highly correlated data. The
132 determined abundance vector w is further used for each pixel representation at the classification
133 process. Then, the abundance representations resulting from *BiICE* are fed to the classification
134 process.
135

136 2.2.5. C. Classification

137 The classification is carried out in both supervised and unsupervised terms. Sepcifically, for the
138 former case the nearest-neighbour classifier (*NN*) is employed, where every training example is
139 stored with its label and a prediction is made for a test example by computing its distance to every
140 training example. In addition to *NN*, *SVMs* are also utilized since they show, in general, superior
141 performance to other classification methods. The advantage of *SVM* is that it successfully works with
142 small number of training samples. Finally, for the unsupervised case, a clustering algorithm, called
143 online adaptive possibilistic c-means (*OAPCM*), is exploited [9]. In *OAPCM*, pixels are being
144 processed one by one and their impact is memorized to suitably defined parameters. Hence, the
145 algorithm is flexible in tracking variations during the clustering formation. *OAPCM* starts with a zero
146 number of clusters and during evolution it creates new clusters or merges existing ones.

147 Figure 3 depicts a flowchart of the two case studies: A) spectral signatures classification and B)
148 abundances representation classification.



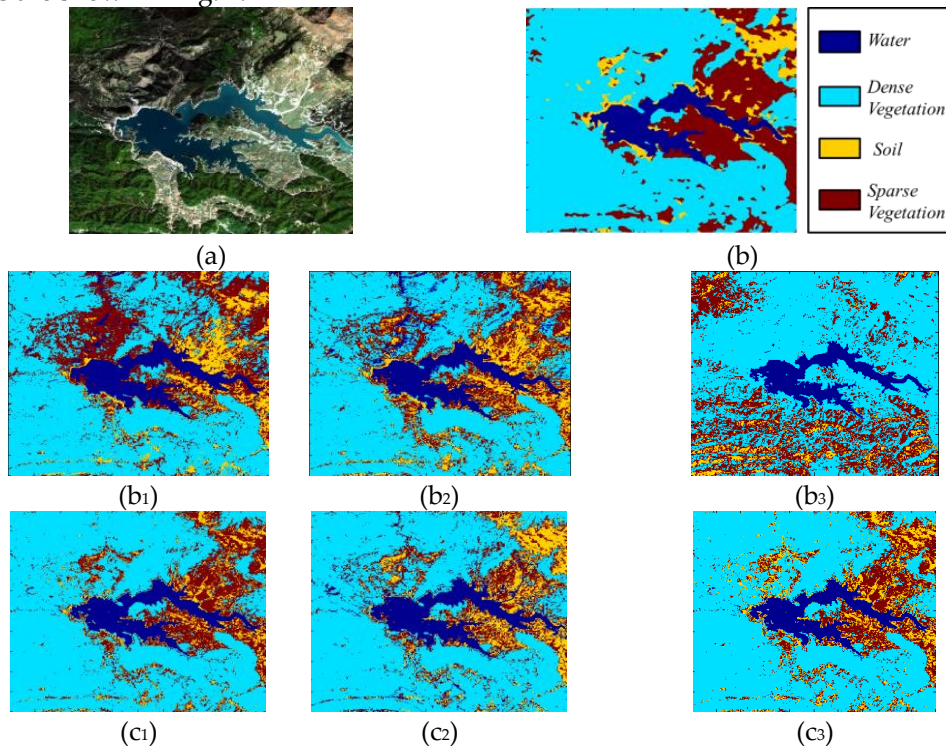
149

150 **Figure 3.** Flowchart of the two case studies: A) spectral signatures classification (red line), B)
151 abundances representation classification (blue line).

152 **3. Results and Discussion**

153 Aiming at a quantitative evaluation, ad-hoc classification approaches proposed in literature such
154 as the nearest neighbor (*NN*) classifier, the support vector machines (*SVMs*) and the unsupervised

155 *OAPCM* algorithm are utilized. The obtained results (classification maps) are validated in terms of
 156 accuracy based on the obtained confusion matrix as can be seen in Tables I and II. In both cases of
 157 supervised classification (*NN*, *SVM*), the four endmembers extracted in the *EE* process are used to
 158 train the classifiers whereas the remaining pixels are used for validation. It should be noted that, in
 159 the case where the abundances representations are used as input for classification, spectral unmixing
 160 is applied on the four endmembers as well as on the remaining pixels. The abundances
 161 representations are used to train the classifiers. As a result, classification maps are generated,
 162 providing information of the area of each land class. The classification utilizing the abundances
 163 representation (*see* Fig.3 case study *B*) achieves an average accuracy which is higher to the
 164 classification that utilizes the spectral signatures (*see* Fig. 3 case study *A*). The water and soil classes
 165 are successfully identified by the two case studies since the average classification accuracies are
 166 similar. However, the dense vegetation and sparse vegetation classes are not successfully identified.
 167 Results are shown in Fig. 4.



168 **Figure 4.** (a) Band 8th of the Sentinel-2 image, (b) Reference map of four classes: water, vegetation,
 169 bare soil and soil-vegetation, (b₁), (b₂), (b₃) classification results obtained by *NN*, *SVM*, *OAPCM*
 170 on spectral signatures, (c₁), (c₂), (c₃) classification results obtained by *NN*, *SVM*, *OAPCM*
 171 on abundances representation.
 172

173 **TABLE I** Comparative Results of Classification Algorithms in Terms of AA for Spectral Signatures

	<i>Water</i>	<i>Dense vegetation</i>	<i>Bare Soil</i>	<i>Sparse vegetation</i>
<i>NN</i>	93,49	80,44	86,86	76,26
<i>SVM</i>	93,16	80,90	87,25	76,77
<i>OAPCM</i>	94,89	55,25	86,41	65,99

174
 175
 176
 177

178
179
180

TABLE II Comparative Results of Classification Algorithms in Terms of AA for Abundances Representation

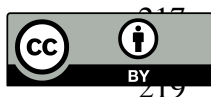
	<i>Water</i>	<i>Dense vegetation</i>	<i>Bare Soil</i>	<i>Sparse vegetation</i>
NN	94,68	86,39	87,12	82,04
SVM	94,90	84,73	88,00	79,41
OAPCM	96,81	86,20	87,79	80,65

181 **4. Conclusion**

182 The objective of this study is to assess the performance of a methodology that has been
183 successfully applied on hyperspectral data on Sentinel-2 data when supervised and unsupervised
184 classification approaches are employed. The advantage of this methodology is that it integrates the
185 abundances representation instead of the basic spectral signatures representation of the pixels. The
186 abundances representation provides sub-pixel level information and in principle is capable of a more
187 accurate mapping of land cover. The adopted methodology has been experimentally evaluated on a
188 Sentinel-2 image of Northern Pindos National Park (Greece) which comprises water, vegetation
189 (dense and sparse) and bare soil areas. The performance of (two supervised and one unsupervised)
190 classification algorithms proposed in literature utilizing the abundance representations is compared
191 with the ones utilizing the spectral signatures in terms of accuracy. The experimental results
192 demonstrate that the proposed algorithm is able to (a) correctly estimate the abundance vectors using
193 a sparsity promoting unmixing scheme that produces the relevant abundance maps and (b) generate
194 more accurate classification maps based on the available reference map.

195 **References**

- 196 1. S. Theodoridis & K. Koutroumbas. Pattern Recognition. Fourth edition, Academic Press.
197 2. E. Mylona, O. Sykioti, K. Koutroumbas, A. Rontogiannis, "Spectral unmixing-based clustering of high-
198 spatial resolution hyperspectral imagery", IEEE Journal of Selected Topics in Applied Earth Observations
199 and Remote Sensing, vol. 10, no 8, pp. 3711-3721, 2017.
200 3. R.A. Topaloglu, E. Sertel and N. Musaoglu, "Assessment of classification accuracies of Sentinel-2 and
201 Landsat-8 data for land cover/use mapping," The International Archives of the Photogrammetry, Remote
202 Sensing and Spatial Information Sciences, vol. XLI-B8, 2016.
203 4. G. Fulop, "Performance of Sentinel-2 data in unsupervised classification: a case study of statistical
204 comparison with Landsat 8 OLI," Journal of Agricultural Informatics, vol. 7 no. 1, pp. 1-12, 2016.
205 5. O. Boiman, E. Shechtman and M. Irani, "In defense of nearest-neighbour based image classification," IEEE
206 Conference on Computer Vision and Pattern Recognition, 2008.
207 6. S. Stagakis, T. Vanikiotis and O. Sykioti, Mapping tree species distribution in a mixed forest through linear
208 unmixing of CHRIS/PROBA imagery, Stagakis, ISPRS Journal of Photogrammetry and Remote Sensing,
209 vol. 119, pp. 79-89, 2016.
210 7. I. Steinwart and A. Christmann. Support Vector Machines. Springer, 2008.
211 8. K.E. Themelis, A.A. Rontogiannis and K.D. Koutroumbas, "A novel hierarchical Bayesian approach for
212 sparse semi-supervised hyperspectral unmixing," IEEE Transactions on Signal Processing, vol. 60, no. 2,
213 pp. 585-599. 2012.
214 9. S.D. Xenaki, K.D. Koutroumbas and A.A. Rontogiannis, "Hyperspectral image clustering using a novel
215 efficient online possibilistic algorithm," 24th European Signal Processing Conference (EUSIPCO), pp. 2020-
216 2024, 2016.



© 2017 by the authors; licensee MDPI, Basel, Switzerland. This article is an open access article distributed under the terms and conditions of the Creative Commons Attribution (CC-BY) license (<http://creativecommons.org/licenses/by/4.0/>).

220